

# Influence of high-pressure torsion on microstructural evolution in an Al–Zn–Mg–Cu alloy

Zhi Chao Duan · Xiao Zhou Liao · Megumi Kawasaki · Roberto B. Figueiredo · Terence G. Langdon

Received: 10 February 2010 / Accepted: 8 March 2010 / Published online: 27 March 2010  
© Springer Science+Business Media, LLC 2010

**Abstract** A commercial age-hardenable Al-7136 alloy was successfully processed by high-pressure torsion (HPT) at room temperature through 1/8 to 4 turns. Microhardness measurements showed significant hardening even after 1/8 turn with the average hardness value reaching a maximum after 1 turn and then slowly decreasing. Higher hardness values were attained by processing the alloy through one pass of equal-channel angular pressing in a supersaturated condition at room temperature and then applying HPT for 1 or 2 turns. Microstructural observations revealed the possibility of achieving true nanometer grain sizes of <100 nm after processing at room temperature. There were variations in hardness with imposed strain due to the fragmentation and subsequent growth of precipitates during processing.

## Introduction

Processing through the application of Severe Plastic Deformation [1], in procedures, such as equal-channel

angular pressing (ECAP) [2] and high-pressure torsion (HPT) [3], has proven exceptionally effective in refining the structure of bulk metallic materials to grain sizes that are generally smaller than ~1 μm. There are numerous scientific reports describing the strengthening and excellent grain refinement that may be achieved when processing disks by HPT [4–8]. However, since a rigid-body analysis predicts that the imposed strain correlates directly with the distance from the center of the disk, it is reasonable to anticipate that the microstructures achieved in HPT will be very heterogeneous. Accordingly, much attention has been devoted to examining the potential for achieving homogeneity across HPT disks.

Several recent experimental studies suggest there is a potential in many materials for achieving a gradual evolution into a reasonably homogeneous microstructure with increasing numbers of revolutions [9–20]. The transition towards a stable microstructure with increasing strain suggests there is a saturation grain size associated with the structural refinement [21]. Furthermore, the structural evolution has been successfully modeled using strain gradient plasticity theory [22, 23]. Despite this success, most of the experimental studies have used high-purity metals or relatively simple metallic alloys and there has been relatively little attention devoted to the evolution of homogeneity in more complex alloys where ageing treatments and precipitation kinetics may be important.

The present investigation was initiated to evaluate the evolution of homogeneity in a commercial Al–Zn–Mg–Cu (Al-7136) alloy using a combination of hardness measurements and microstructural observations. There are several earlier reports describing the processing and characteristics of this alloy when using ECAP [24–27].

Z. C. Duan (✉) · M. Kawasaki · T. G. Langdon  
Departments of Aerospace & Mechanical Engineering  
and Materials Science, University of Southern California,  
Los Angeles, CA 90089-1453, USA  
e-mail: zduan@usc.edu

X. Z. Liao  
School of Aerospace, Mechanical and Mechatronic Engineering,  
University of Sydney, Sydney, NSW 2006, Australia

R. B. Figueiredo · T. G. Langdon  
Materials Research Group, School of Engineering Sciences,  
University of Southampton, Southampton SO17 1BJ, UK

## Experimental material and procedure

The experiments were conducted using a commercial Al-7136 alloy obtained from QED Inc. (San Diego, CA). The alloy was provided in the form of extruded rods having diameters of 10.0 mm. The Al-7136 alloy is an Al-Zn-Mg-Cu alloy and a chemical analysis gave a composition, in wt%, of 9.4% Zn, 2.5% Mg, and 2.5% Cu with additions of 0.12% Si, 0.15% Fe, 0.2% Zr, 0.05% Mn, 0.05% Cr, and 0.1% Ti. Disks having thicknesses of ~1.5 mm were cut from the rods and then carefully polished with methanol to a final thickness of ~0.8 mm.

The disks were processed by HPT at room temperature using a facility having upper and lower anvils made from high-strength YXR3 tool steel and with nitrided surfaces. Each anvil was machined with a spherical depression at the center having a depth of 0.25 mm and a diameter of 10 mm. The sample disk was placed in the depression on the lower anvil and this anvil was then brought upwards and into position so that the disk was contained within the depressions on the two anvil surfaces. Processing was conducted using an applied pressure,  $P$ , of 6 GPa and with concurrent torsional straining applied to the disk by rotation of the lower anvil. The rotation speed for all tests was 1 rpm and the disks were strained through numbers of turns,  $N$ , from 1/8 to 4.

In order to change the grain size and the precipitation morphologies in some of the disks before processing by HPT, some samples were initially processed by ECAP. Following the procedure developed earlier for successful pressing of the Al-7136 alloy [27], these samples were given a solution treatment at 743 K for 1 h, water quenched to introduce a supersaturated solid solution, and then naturally aged for ~10 min at room temperature prior to processing by ECAP. Earlier experiments showed that the Al-7136 alloy may be pressed at 473 K for up to eight passes without the occurrence of any cracking or segmentations [24, 25], but there is a subsequent loss of strength by comparison with the as-received alloy [27]. In practice, this loss of strength may be avoided by making use, as in the present experiments, of an appropriate solid solution treatment followed by water quenching, and immediate processing by ECAP at room temperature [27, 28]. The ECAP was conducted using a solid die with an internal channel angle of  $\Phi = 90^\circ$  and an outer arc of curvature of  $\psi \approx 20^\circ$ . It can be shown that these values of  $\Phi$  and  $\psi$  lead to an imposed strain of ~1 in a single pass [29]. Disks were sectioned from these ECAP billets, polished to thicknesses of ~0.8 mm and then strained by HPT through totals of either 1 or 2 turns.

Following HPT, the distorted layers of all disks were removed gently by polishing with soft cloths to give smooth and mirror-like surfaces. The values of the Vickers microhardness,  $H_V$ , were then systematically recorded using

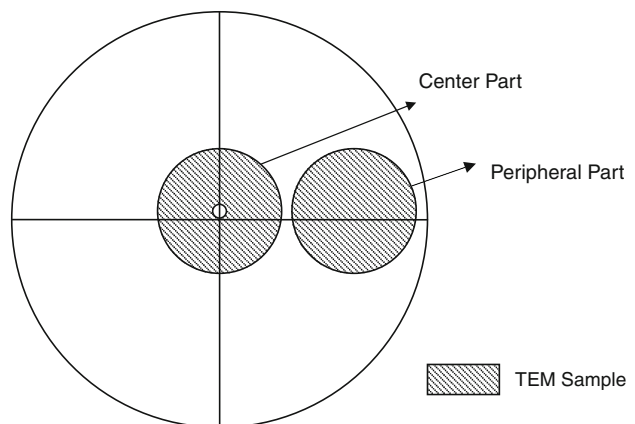


**Fig. 1** Partition of the HPT disk for TEM investigation

an FM-1e microhardness tester with a load of 100 gf and a dwell time for each measurement of ~15 s. An earlier report described the two procedures for taking these hardness measurements [16]. Specifically, measurements were initially taken along a diameter of each disk at positions separated by 0.3 mm and with four separate hardness measurements recorded at each position by taking measurements uniformly spaced around the selected position and at a distance of 0.15 mm. Second, measurements were taken over the total surface of each disk following a rectilinear grid pattern with a separation of 0.3 mm between each point and these measurements were used to construct color-coded contour maps which provide a clear visual presentation of the variations in hardness across each disk.

The microstructures were recorded after HPT using transmission electron microscopy (TEM). Each disk was divided into two parts where the center part was a concentric disk of 3-mm diameter centered very close to the center of the sample and the peripheral part was a disk of 3-mm diameter situated between the center and the edge of the sample: these locations are shown in Fig. 1. The TEM samples were extracted after thinning each disk to an overall thickness of ~100  $\mu\text{m}$ . The 3-mm disks were then thinned using a twin-jet electropolishing unit with an electrolyte of 30% nitric acid and 70% methanol at 20 V and a polishing temperature of -20 °C. Bright-field images were recorded at different magnifications using a Philips CM12 microscope operating at 120 kV.

## Experimental results

Microhardness study of the Al-7136 alloy after HPT and ECAP + HPT

Figure 2 shows the values of  $H_V$  recorded along diameters of each disk where (a) is for HPT through values of  $N$  of

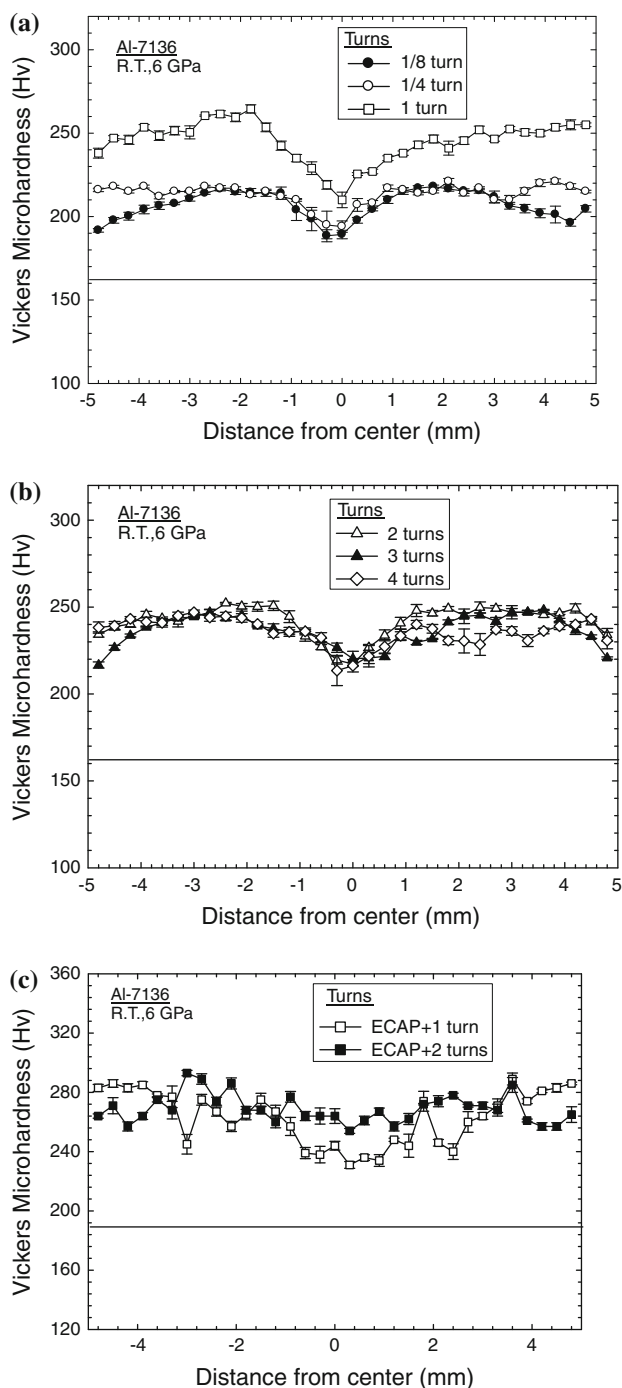


**Fig. 2** Vickers microhardness,  $H_v$ , versus distance from the center of the disk after **a** HPT through 1/8 to 1 turn, **b** HPT through 2–4 turns, and **c** ECAP + HPT through 1 and 2 turns

1/8, 1/4 and 1 turn, (b) is for HPT through 2, 3 and 4 turns, and (c) is for samples subjected to ECAP and then HPT through 1 and 2 turns: the error bars represent the 95% confidence limits in each plot, the lower horizontal lines in (a) and (b) show the measured value of  $H_v$  before HPT and the lower horizontal line in (c) shows the value of  $H_v$  after

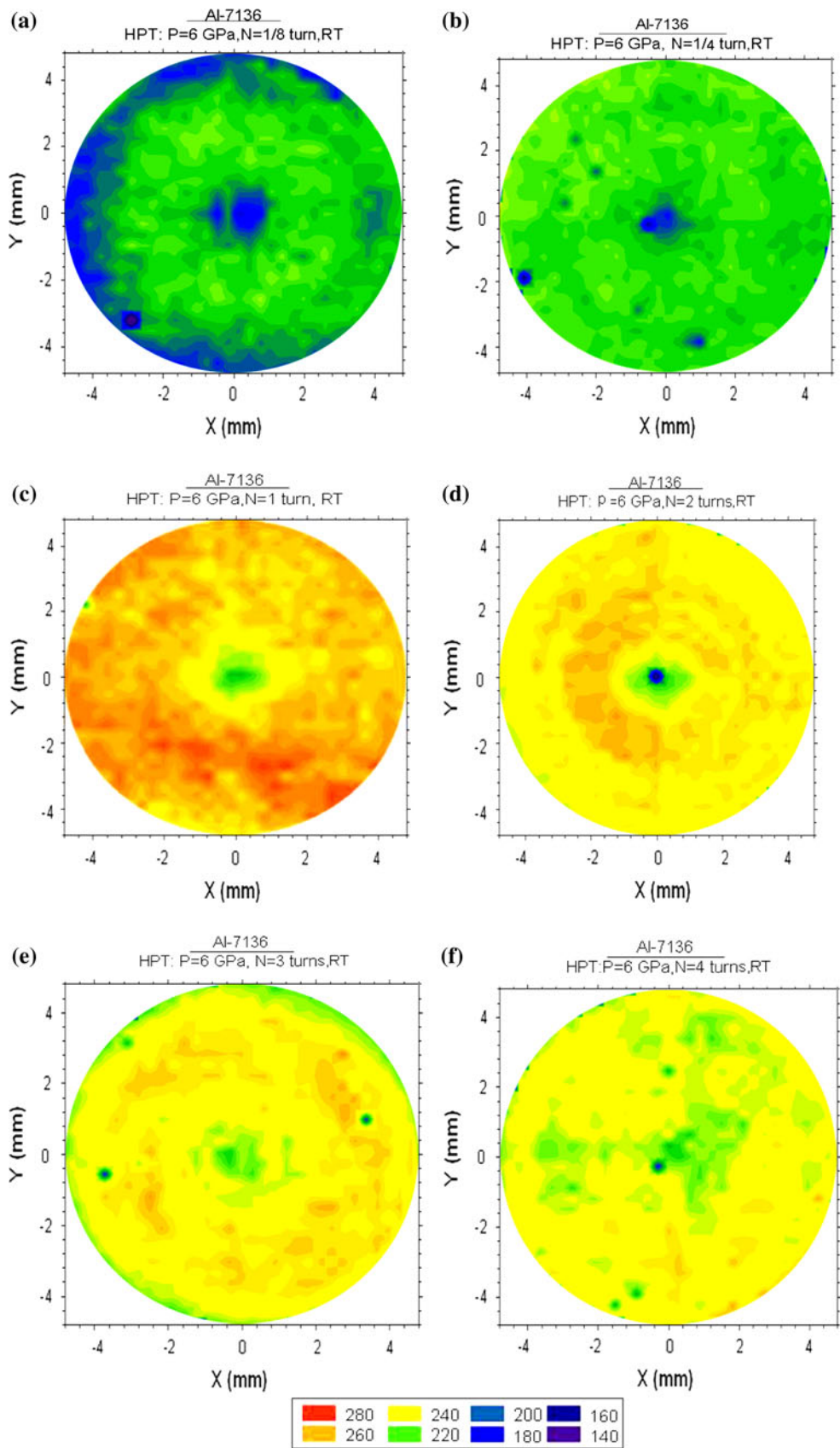
ECAP but prior to HPT. Three conclusions may be reached from inspection of the experimental data. First, there is a very significant increase in hardness after only 1/8 turn and the hardness continues to increase up to  $\sim 1$  turn. Second, the values of  $H_v$  tend to be lower in the center of the disk and this is similar to earlier results for the Al-6061 alloy [15, 17] but different to the results for high-purity aluminum where higher hardness values were recorded in the centers of the disks due to rapid recovery in the peripheral regions [13]. Third, although there is significant scatter in the individual datum points, the average hardness values are higher after processing by ECAP followed by HPT as shown in Fig. 2c.

In order to provide a macroscopic representation of the variations in hardness across the total surfaces of the disks, Fig. 3 shows the color-coded contour maps for disks processed by HPT through totals of (a) 1/8, (b) 1/4, (c) 1, (d) 2, (e) 3, and (f) 4 turns, respectively: in these maps,  $X$  and  $Y$  denote two arbitrary orthogonal axes marked in mm with the positions (0,0) located at the centers of each disk.

The maps in Fig. 3 demonstrate there is an initial increase in hardness from 1/8 to 1 turn with lower values of  $H_v$  around the center of the disk but thereafter, at even higher numbers of revolutions, the results are unusual because there is a slow but measurable loss in hardness. Thus, in Fig. 3a after 1/8 turn the majority of the datum points fall in the range of  $H_v$  from 200 to 220 with a weaker region in the center of the disk where the average Vickers hardness is  $\sim 180$ –190. In Fig. 3b after 1/4 turn the outer weaker region has disappeared and the central weaker region has also decreased in size. Increasing to 1 turn in Fig. 3c, there is now significant strengthening with an average value of  $H_v$  approaching  $\sim 250$  and a weaker center where the hardness is  $\sim 200$ –220. A maximum hardness was recorded in this condition with some individual values of  $H_v$  up to  $\sim 280$ . After 2 turns in Fig. 3d, the hardness no longer continues to increase but rather it decreases with an average value of  $\sim 240$  and with a weaker central region that remains essentially unchanged in size and magnitude. There is a gradual continuation in the decrease in hardness with additional straining as shown in Fig. 3e for 3 turns and Fig. 3f for 4 turns. It is evident after 4 turns that the lowest values of  $H_v$  in the central region remain essentially unchanged when processing through 1–4 passes, whereas the higher hardness values around the periphery decrease towards a saturation value of the order of  $H_v \approx 220$ .

Adopting a procedure introduced earlier for studying hardness evolution in samples processed by ECAP [30], it is convenient to present the hardness data collected across each disk in the form of histograms showing the number fractions of the individual microhardness values plotted against the values of  $H_v$  in increments of 20. These plots

**Fig. 3** Color-coded contour maps showing the distributions of hardness values across disks processed by **a** 1/8 turn, **b** 1/4 turn, **c** 1 turn, **d** 2 turns, **e** 3 turns, and **f** 4 turns: the significance of the colors is shown in the color key at the bottom (Color figure online)



are shown in Fig. 4 for the six testing conditions of (a) 1/8, (b) 1/4, (c) 1, (d) 2, (e) 3, and (f) 4 turns, respectively, where the average of  $H_v$  is denoted in each plot by a vertical line. Two conclusions may be drawn from these plots. First, the average hardness initially increases

substantially up to  $\sim 1$  turn and then slowly decreases at larger numbers of revolutions. This is shown more directly in Fig. 5 where the average hardness is plotted against the number of turns. Second, the width of the distribution is a minimum after 1/4 turn but the width increases again at

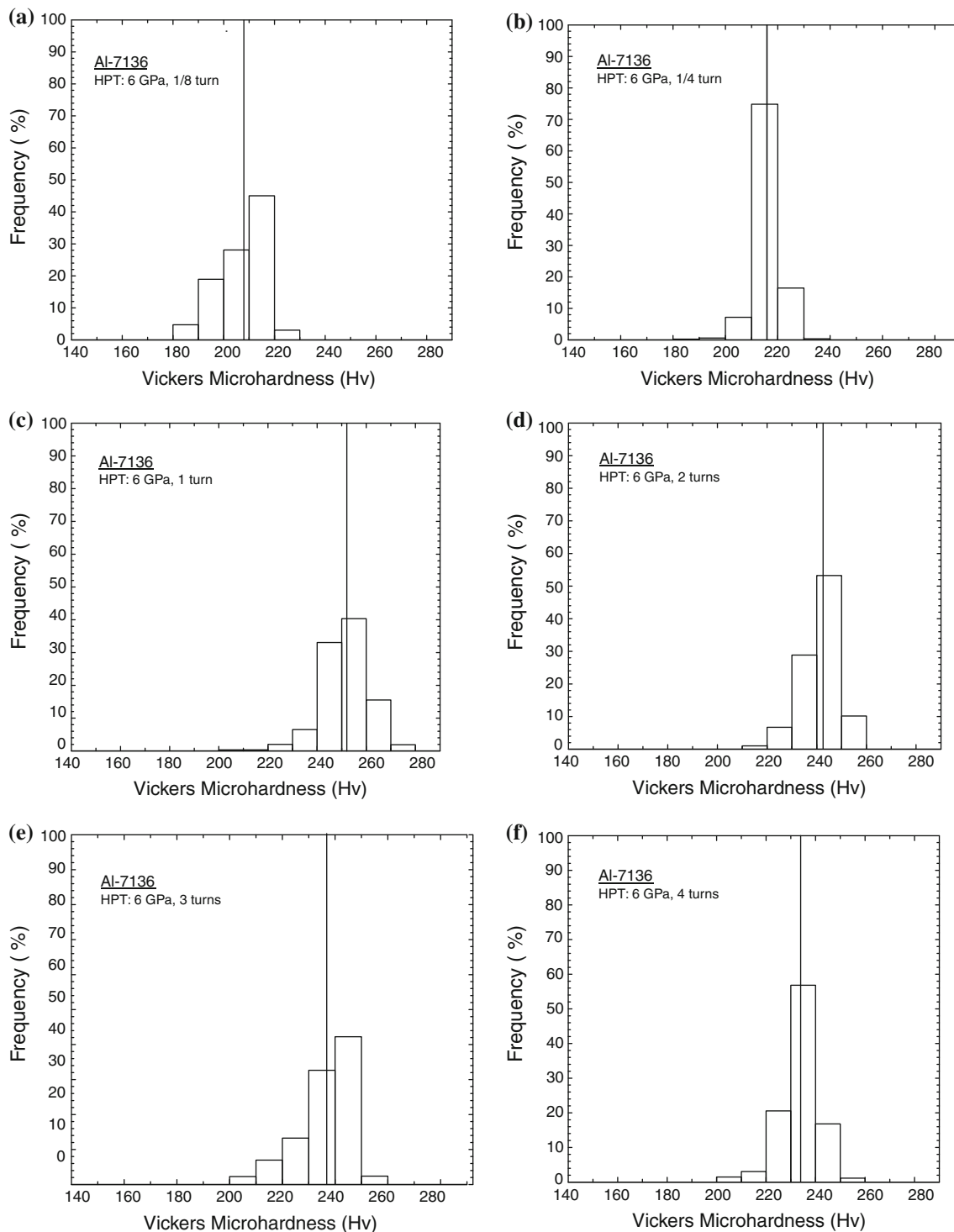


**Fig. 4** Histograms of the Vickers microhardness values after HPT through **a** 1/8 turn, **b** 1/4 turn, **c** 1 turn, **d** 2 turns, **e** 3 turns, and **f** 4 turns: the vertical lines denote the average values

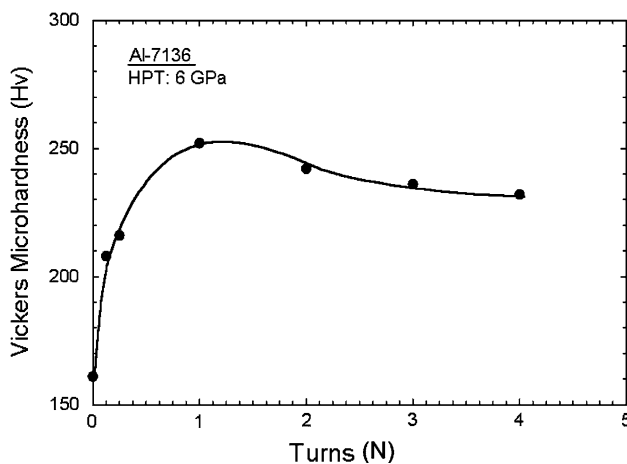


**Fig. 5** Variation of the average Vickers microhardness,  $H_v$ , with number of turns of HPT,  $N$

1 turn and remains similar up to 4 turns. At  $N = 1/4$  turn where there is optimum homogeneity, more than 70% of the values of  $H_v$  fall between 210 and 220.

The additional strengthening achieved using HPT is also readily apparent from Fig. 6 which shows the color-coded maps and the hardness distribution histograms after ECAP for 1 pass and HPT through 1 turn in Fig. 6a and b and HPT through 2 turns in Fig. 6c and d. After 1 turn in Fig. 6a, the average hardness value is  $H_v \approx 275$  which is significantly higher than  $H_v \approx 252$  for 1 pass of HPT in Fig. 4c. Similarly, after 2 turns in Fig. 6c the average hardness is  $H_v \approx 270$  which is higher than the value of  $H_v \approx 242$  after 2 passes in Fig. 4d. The color-coded maps in Fig. 6 reveal also some differences by comparison with the samples processed only by HPT because the area in the vicinity of the central part of the disk increases in hardness between 1 and 2 turns, whereas the peripheral region decreases in hardness over the same range of torsional straining. A second observation is that the spread of the histograms is larger in Fig. 6 than for the samples processed only by HPT in Fig. 4.

#### Microstructures of the Al-7136 alloy after HPT and ECAP + HPT

An earlier report described the microstructure in the as-received Al-7136 alloy [24]. In this condition there was a low dislocation density and the grains were reasonably equiaxed with an average size of  $\sim 3.4 \mu\text{m}$ . There were plate-shaped  $\eta$  precipitates within the grains having lengths of  $\sim 600\text{--}800 \text{ nm}$  and widths of  $\sim 200 \text{ nm}$  and there were also needle-like  $\eta'$  phases lying predominantly along the grain boundaries and having lengths of  $<40 \text{ nm}$ .

Figure 7 shows two representative microstructures near the edges of the disks after straining through (a) 1 turn and

(b) 4 turns, respectively. After rotation through 1 turn, there was a high dislocation density in the center of the disk but the grains were equiaxed with an average size of  $\sim 200 \text{ nm}$ . The central region also contained aligned arrays of precipitates with sizes of  $\sim 10\text{--}20 \text{ nm}$ . The absence of the larger  $\eta$  precipitates after 1 turn and the alignment of the small precipitates is evidence for fragmentation of the larger particles during torsional straining. In the peripheral part of the 1-turn sample the grains were equiaxed, as shown in Fig. 7a, and the measured average grain size was  $\sim 120 \text{ nm}$ . This smaller grain size by comparison with the central region is consistent with the hardness distribution shown in Fig. 3c. It was observed also that there was little evidence for arrays of aligned precipitates in this peripheral region although there were some slightly larger precipitates distributed along the grain boundaries. This is consistent with earlier observations of the fragmentation of  $\eta$ -phase precipitates in an Al-7034 alloy processed by ECAP [31].

After straining through 2 turns, the average grain size in the central part was  $\sim 150 \text{ nm}$  but the precipitates were larger at  $\sim 25\text{--}30 \text{ nm}$  and distributed mainly along the grain boundaries. In the peripheral region of this sample the grain size was  $\sim 100 \text{ nm}$  which showed a further reduction in grain size but with precipitates of  $\sim 25\text{--}30 \text{ nm}$  demonstrating an increase in precipitate size between 1 and 2 revolutions. This increase in precipitate size between 1 and 2 turns reduces the numbers of obstacles to dislocation movement and this provides a direct explanation for the small decrease in hardness evident in Fig. 3d and as recorded in Fig. 5.

Inspection of the sample processed through 4 turns, as shown in Fig. 7b, showed two different populations of grain sizes in the peripheral region. Specifically, there were some small grains of  $\sim 90\text{--}100 \text{ nm}$  which were similar in size to the sample processed through 2 turns but there were also some larger grains with average sizes of  $\sim 170 \text{ nm}$ . The largest individual grain sizes recorded in this condition were  $\sim 300 \text{ nm}$ . These measurements suggest the occurrence of dynamic recovery or recrystallization during processing to a higher strain because no large grains were observed in the samples processed through 1 or 2 turns. The development of larger grains at high strains was noted earlier in samples of high-purity aluminum processed through 12 passes of ECAP [32]. The precipitate sizes were also different after 4 turns with the presence of some larger precipitates at  $\sim 40 \text{ nm}$  which further reduces the numbers of obstacles to dislocation movement.

For the samples subjected to ECAP followed by HPT, representative microstructures are shown in Fig. 8 in the edge region after 1 turn of HPT and in Fig. 9 after 2 turns of HPT for (a) the center and (b) the edge. For ECAP + 1 turn of HPT as shown in Fig. 8, the microstructure in the peripheral region of the disk was well defined with

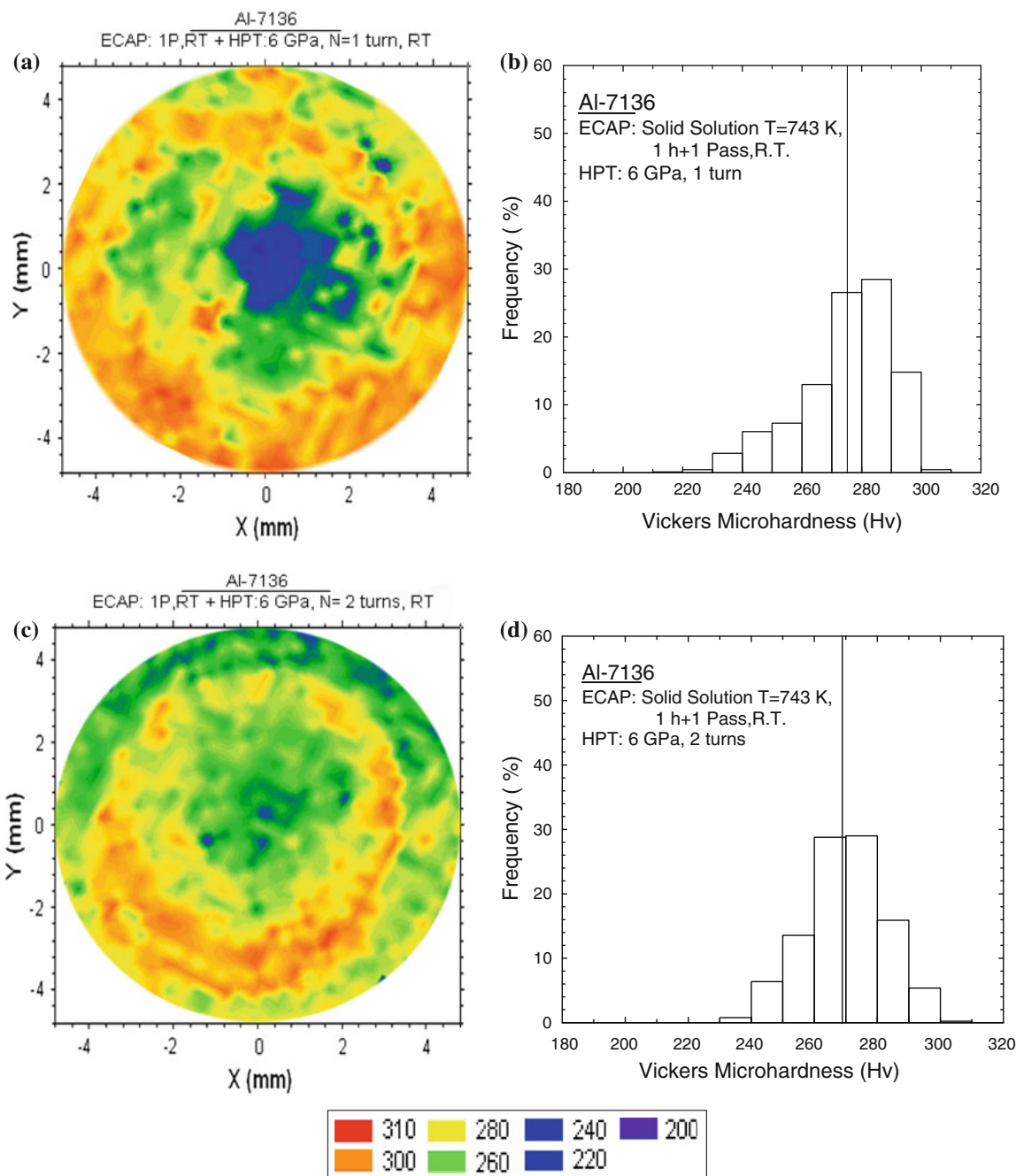


**Fig. 6** Color-coded contour maps and histograms showing the distributions of hardness values across disks processed by ECAP + HPT for **a, b** 1 turn and **c, d** 2 turns: the significance of the colors is shown in the color key at the bottom (Color figure online)

equiaxed grains having an average size of  $\sim 80$  nm and with very small precipitates of  $\sim 10$  nm distributed primarily on the grain boundaries. For the ECAP + 2 turns sample, the central region shown in Fig. 9a was similar to the edge region after a single turn with equiaxed grains having an average size of  $\sim 70\text{--}80$  nm and small precipitates on the boundaries with average sizes of  $\sim 10$  nm. For the peripheral region of this sample shown in Fig. 9b, the

measured average grain size was  $<40$  nm although the precipitates remained with sizes of  $\sim 10$  nm.

## Discussion

The age-hardenable Al-7136 alloy is not easy to process by ECAP at room temperature because of the occurrence of

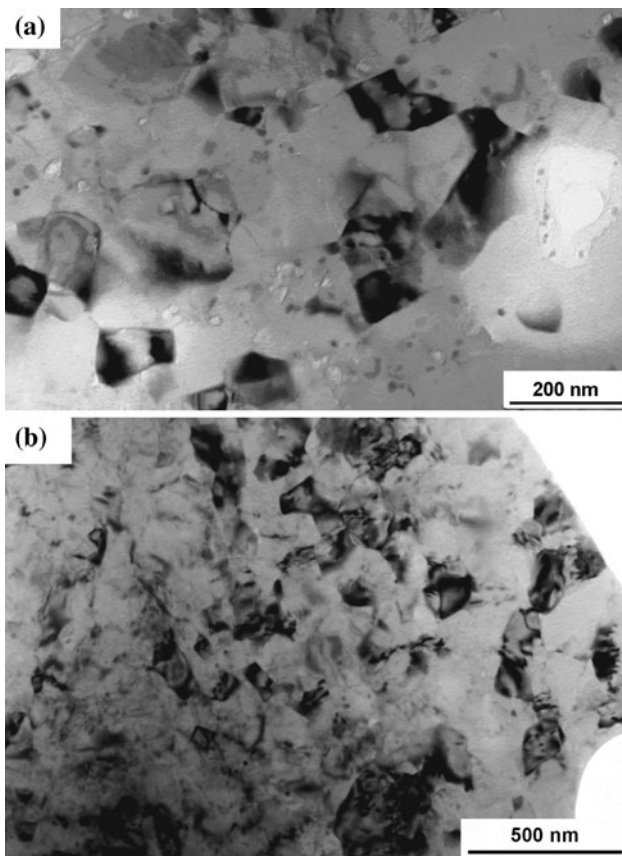


**Fig. 7** Microstructures in the peripheral regions of disks processed by HPT through **a** 1 turn and **b** 4 turns

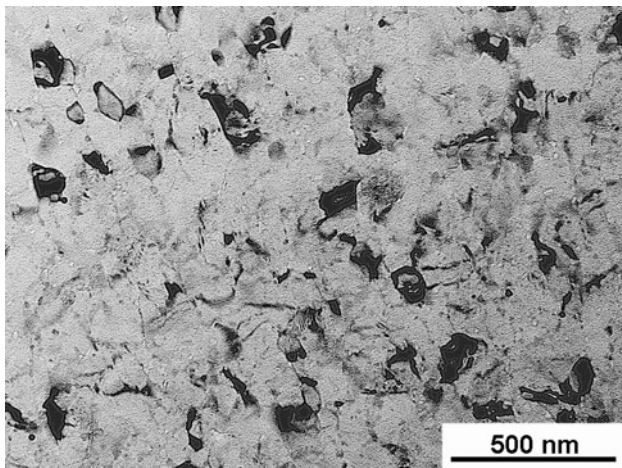


**Fig. 8** Microstructure in the peripheral region of a disk processed by ECAP + HPT through 1 turn

cracking and segmentation [27]. It has been shown that this problem may be avoided using a strategy in which the material is subjected to a solution treatment and water quenching to produce a supersaturation and then performing the ECAP immediately after quenching [27, 28]. However, despite this inherent difficulty with ECAP, the

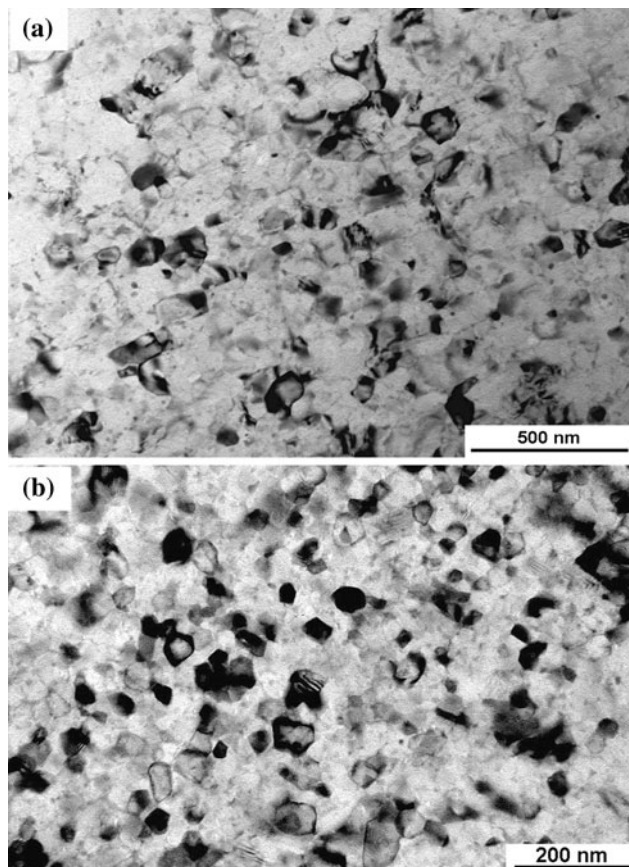


**Fig. 9** Microstructures in disks processed by ECAP + HPT through 2 turns **a** in the center and **b** in the peripheral region

present results show that the as-received Al-7136 alloy may be successfully processed by HPT at room temperature without the introduction of any cracking and, furthermore, this processing gives significant strengthening as recorded in Figs. 2 and 3. It is also important to note that HPT leads to a very high level of strengthening even after processing for only 1/8 turn as shown in Fig. 5. The result at a low level of torsional straining is consistent with other experimental data obtained using both disk [20, 33–35] and ring [35–37] samples.

Processing by ECAP for 1 pass in a supersaturated condition and then torsionally straining in HPT introduces even more strengthening by comparison with HPT processing of the as-received material. This is evident from inspection of Fig. 6. The additional strengthening achieved by conducting the HPT after processing by ECAP is consistent with the presence of a supersaturated condition. It also matches the smaller grain sizes reported earlier both in various samples processed by a combination of ECAP and HPT [38, 39] and in experiments where HPT was preceded by preliminary processing using other techniques such as electro-deposition, ball milling, or rapid quenching [40]. In addition, the measured average grain sizes of ~80 nm

after ECAP + 1 HPT turn and <40 nm after ECAP + 2 HPT turns provide a clear demonstration that it is possible to use room temperature processing of ECAP combined with HPT to achieve a true nanostructured condition in the Al-7136 alloy.

In practice, there are several experimental parameters affecting the nature of grain refinement and microstructural evolution when processing by HPT [41]. Nevertheless, the present results show that very significant microstructural refinement is achieved even in a complex commercial alloy such as Al-7136. The processing by severe plastic deformation of supersaturated solid solutions requires a balance between deformation-induced disordering and deformation-accelerated diffusion that will bring the alloys closer to an equilibrium condition. It is well established that an increase in the concentration of the solute component leads to solid solution hardening, whereas a decrease in grain size gives hardening. Accordingly, these two processes will compete in the present alloy system.

Earlier reports using 3-D atom tomography on samples of the Al-7136 alloy processed by ECAP revealed the segregation of alloying elements to the grain boundaries after processing by ECAP combined with an accelerated growth of precipitates suggesting that dislocations may serve as fast diffusion paths [24, 25]. Since HPT is a more intense processing mode than ECAP, generally leading to smaller grain sizes and higher dislocation densities, it is reasonable to anticipate these characteristics of segregation and diffusion will exist also in the samples processed by HPT. This faster diffusion would be assisted by the presence of a higher vacancy concentration after HPT where these vacancies are introduced during the heavy straining process. This suggestion is supported by several reports documenting increased vacancy concentrations after processing by compression [42], ECAP [43], and HPT [44].

## Summary and conclusions

1. A commercial age-hardenable Al-7136 alloy was successfully processed at room temperature using two different processing procedures by: applying HPT to the as-received extruded alloy and combining 1 pass of ECAP for the supersaturated alloy and then processing by HPT. Both procedures gave excellent results without any cracking.
2. Microhardness measurements were taken after HPT on disks subjected to a range of torsional strains from 1/8 turn to 4 turns. For the as-received alloy processed by HPT, there was significant strengthening after 1/8 turn and the hardness values increased to a maximum after 1 turn and thereafter there was a small decrease in hardness. After processing by ECAP and HPT, the

disks exhibited higher levels of hardness due to the initial presence of a supersaturated condition.

3. True nanometer grain sizes of <100 nm were achieved in this alloy after a combination of ECAP and HPT. The results show that the variation of hardness with imposed strain is primarily a consequence of the fragmentation and subsequent growth of precipitates during the processing operation.

**Acknowledgement** This study was supported by the National Science Foundation of the United States under Grant No. DMR-0855009.

## References

1. Valiev RZ, Islamgaliev RK, Alexandrov IV (2000) *Prog Mater Sci* 45:103
2. Valiev RZ, Langdon TG (2006) *Prog Mater Sci* 51:881
3. Zhilyaev AP, Langdon TG (2008) *Prog Mater Sci* 53:893
4. Sergueeva AV, Stolyarov VV, Valiev RZ, Mukherjee AK (2001) *Scripta Mater* 45:747
5. Valiev RZ, Sergueeva AV, Mukherjee AK (2003) *Scripta Mater* 49:669
6. Wei Q, Zhang HT, Schuster BE, Ramesh KT, Valiev RZ, Kecske LJ, Dowding RJ, Magness L, Cho K (2006) *Acta Mater* 54:4079
7. Lugo N, Llorca N, Cabrera JM, Horita Z (2008) *Mater Sci Eng A* 477:366
8. Murashkin MYu, Kil'mametov AR, Valiev RZ (2008) *Phys Met Metal* 106:90
9. Zhilyaev AP, Nurislamova GV, Kim BK, Baró MD, Szpunar JA, Langdon TG (2003) *Acta Mater* 51:753
10. Vorhauer A, Pippal R (2004) *Scripta Mater* 51:921
11. Zhilyaev AP, Ohishi K, Langdon TG, McNelley TR (2005) *Mater Sci Eng A* 410–411:277
12. Pippal R, Vorhauer A, Wetscher F, Faleschini M, Hafok M, Sabirov I (2006) *Mater Sci Forum* 503–504:407
13. Xu C, Horita Z, Langdon TG (2007) *Acta Mater* 55:203
14. Zhilyaev AP, McNelley TR, Langdon TG (2007) *J Mater Sci* 42:1517. doi:[10.1007/s10853-006-0628-0](https://doi.org/10.1007/s10853-006-0628-0)
15. Xu C, Horita Z, Langdon TG (2008) *Acta Mater* 56:5168
16. Kawasaki M, Langdon TG (2008) *Mater Sci Eng A* 498:341
17. Xu C, Horita Z, Langdon TG (2008) *J Mater Sci* 43:7286. doi: [10.1007/s10853-008-2624-z](https://doi.org/10.1007/s10853-008-2624-z)
18. Xu C, Langdon TG (2009) *Mater Sci Eng A* 503:71
19. Kawasaki M, Ahn B, Langdon TG (2010) *Acta Mater* 58:91
20. Xu C, Horita Z, Langdon TG (2010) *Mater Trans* 51:2
21. Pippal R, Wetscher F, Hafok M, Vorhauer A, Sabirov S (2006) *Adv Eng Mater* 8:1046
22. Estrin Y, Molotnikov A, Davies CHJ, Lapovok R (2008) *J Mech Phys Solids* 56:1186
23. Molotnikov A (2008) *Mater Sci Forum* 584–586:1051
24. Sha G, Wang YB, Liao XZ, Duan ZC, Ringer SP, Langdon TG (2009) *Acta Mater* 57:3123
25. Sha G, Ringer SP, Duan ZC, Langdon TG (2009) *Intl J Mater Res* 100:1674
26. Figueiredo RB, Duan Z, Kawasaki M, Langdon TG (2010) *Mater Sci Forum* 633–634:341
27. Duan ZC, Chinh NQ, Xu C, Langdon TG (2010) *Metall Mater Trans A* 41A:802
28. Chinh NQ, Gubicza J, Czepe T, Lendvai J, Xu C, Valiev RZ, Langdon TG (2009) *Mater Sci Eng A* 516:248
29. Iwahashi Y, Wang J, Horita Z, Nemoto M, Langdon TG (1996) *Scripta Mater* 35:143

30. Xu C, Langdon TG (2007) J Mater Sci 42:1542. doi:[10.1007/s10853-006-0899-5](https://doi.org/10.1007/s10853-006-0899-5)
31. Xu C, Furukawa M, Horita Z, Langdon TG (2003) Acta Mater 51:6139
32. Kawasaki M, Horita Z, Langdon TG (2009) Mater Sci Eng A524:143
33. Edalati K, Fujioka T, Horita Z (2008) Mater Sci Eng A497:169
34. Ito Y, Horita Z (2009) Mater Sci Eng A503:32
35. Edalati K, Fujioka T, Horita Z (2009) Mater Trans 50:44
36. Harai Y, Ito Y, Horita Z (2008) Scripta Mater 58:469
37. Edalati K, Horita Z (2009) Mater Trans 50:92
38. Zhilyaev AP, Kim BK, Szpunar JA, Baró MD, Langdon TG (2005) Mater Sci Eng A391:377
39. Zhilyaev AP, Gimazov AA, Raab GI, Langdon TG (2008) Mater Sci Eng A486:123
40. Zhilyaev AP, Gimazov AA, Soshnikova EP, Révész Á, Langdon TG (2008) Mater Sci Eng A489:207
41. Hohenwarter A, Bachmaier A, Gludovatz B, Scheriau S, Pippan R (2009) Int J Mater Res 100:1653
42. Ungár T, Schafler E, Hanák P, Bernstorff S, Zehetbauer M (2005) Z Metallkd 96:578
43. Zehetbauer M, Schafler E, Ungár T (2005) Z Metallkd 96:1044
44. Sauvage X, Wetscher F, Pareige P (2005) Acta Mater 53:2127